Spectral Quantification of Nonlinear Elasticity using Acousto-elasticity and Shear-Wave Dispersion

Spectral Quantification of Nonlinear Elasticity using Acousto-elasticity and Shear-Wave Dispersion

Corin F. Otesteanu, Bhaskara R. Chintada, Marga B. Rominger,
Sergio J. Sanabria, Orcun Goksel

***Abstract*—Tissue biomechanical properties are known to be sensitive to pathological changes. Accordingly, various techniques have been developed to estimate tissue mechanical properties. Shear-wave elastography (SWE) measures shear-wave speed (SWS) in tissues, which can be related to shear modulus. Although viscosity or stress-strain non-linearity may act as confounder of SWE, their explicit characterization may also provide additional information about tissue composition as a contrast modality. Viscosity can be related to frequency dispersion of SWS, which can be characterized using multi-frequency measurements, herein called *spectral shear-wave elastography* (SSWE). Additionally, non-linear shear modulus can be quantified and parameterized based on SWS changes with respect to applied stress; a phenomenon called acousto-elasticity (AE). In this work, we characterize the non-linear parameters of tissue as a function of excitation frequency by utilizing both AE and SSWE together. For this, we apply incremental amounts of quasi-static stress on a medium, while imaging and quantifying SWS dispersion via SSWE. Results from phantom and ex-vivo porcine liver experiments demonstrate the feasibility of measuring frequency-dependent non-linear parameters using the proposed method. SWS propagation in porcine liver tissue was observed to change from 1.8 m/s at 100 Hz to 3.3 m/s at 700 Hz, while increasing by approximately 25% from a strain of 0% to 12% across these frequencies.**

***Index terms*—Ultrasound, elastography, acousto-elasticity, tissue non-linearity, shear-wave dispersion**

I. INTRODUCTION

Early detection of diseases is of high importance for the timely treatment and a positive outcome for the patient. Diseases such as liver fibrosis [1] and steatosis [2], tumors [3], atherosclerosis [4] have been shown to change the biomechanical tissue parameters, when compared to healthy tissue. For this reason, noninvasive methods that characterize tissue mechanical properties are of great interest as they can aid diagnosis and treatment [5].

Ultrasound shear-wave elastography (SWE) is a noninvasive imaging technique in which acoustic radiation force is used to induce shear-waves in tissue. The propagating shear-wave is observed using ultrasound imaging to determine the shear-wave speed (SWS) which is directly related to the underlying tissue shear modulus [6]. This method is currently used in many clinical applications for disease diagnosis, such as liver fibrosis and breast cancer [1], [7]. While having good sensitivity in the case of breast cancer diagnosis, SWE may result in many false positives due to a relatively poorer specificity [8]. Similarly, in the case of liver, challenges in the diagnosis of fibrosis staging may arise, especially at early stages of fibrosis and in patients with steatosis [9]. It has been previously shown that due to its viscosity, tissue exhibits dispersive behavior, which affects SWS measurement accuracy [10], [11]. Moreover, the degree of compression applied to the tissue is a confounder, which was also shown to affect SWS measurements by up to 50% [12].

For a better understanding and diagnosis of pathological changes in tissue, multi-parametric diagnostics are desirable, for which additional tissue biomarkers should also be measured. It was shown previously that mechanical parameters such as viscosity [2], [1] or shear modulus non-linearity [13], [14] can complement shear modulus measurements and aid in early diagnosis. At the same time, their measurement would also diminish the confounding effect they have on SWS. It was shown in [13] that, while benign and malignant breast tumors had similar elastic moduli at low strains, at larger strains the elastic modulus of the malignant lesions elevated up to 2.5 times, because of the non-linear stress—strain response of such tissues [13]. More recently, tissue non-linearity was characterized in a tissue-mimicking phantom using SWE at increasing compression levels by measuring the change in shear-wave velocity due to the acousto-elasticity (AE) phenomenon [15]. This effect describes the change in wave speed propagation as a function of quasi-static stress applied to an elastic and nearly-incompressible body. Based on AE, several studies [16], [17], [18], [19] investigated the non-linear behavior of tissue by quantifying the third order non-linear modulus (cf. [20]). In [16] the non-linear properties of liver samples have been investigated. In a clinical study in [17] it was shown that benign and malignant breast tumors can be differentiated by their non-linear shear modulus. In [18] changes in non-linear modulus was studied in bladder samples before and after treatment with formalin. In [19] the effect of compression area and direction was investigated in kidney samples. Other works employed the Demiray-Fung hyperelastic model to quantify non-linear properties of ex-vivo porcine liver tissue [21] and ex-vivo brain tissue [22]. In these studies, tissue non-linear parameters were characterized at the excitation frequency of the induced shear-wave. However, it was shown in [23], [24] that the non-linear parameters also change with excitation frequency. Therefore, it is essential to study non-linearity also as a function of frequency.

The acoustic radiation force induces an impulsive response (push), which contains a broadband frequency range. Thanks

C.F. Otesteanu, B.R. Chintada, S.J. Sanabria, and O. Goksel are with the Computer-assisted Applications in Medicine (CAiM) group, Swiss Federal Institute of Technology (ETH), Zurich, Switzerland. (email: ogoksel@ethz.ch)

M.B. Rominger is with the Department of Diagnostic and Interventional Radiology, University Hospital of Zurich (USZ), Zurich, Switzerland.

to this large bandwidth of the induced shear-wave, SWS can be characterized at different frequencies using conventional SWE alone by measuring the speed for individual frequencies — without requiring any additional setup or hardware. This has been extensively studied in the literature, and is referred to herein as spectral shear-wave elastography (SSWE). Frequency dependent SWS have been measured in several different ways: e.g. by relating the SWS to the phase shift detected across the propagated distance [25], [26]; by using a 2D Fourier transform of the shear-wave propagation movie [27], [28]; by estimating the relaxation time of an acoustic radiation force induced stress [29]; by estimating the complex shear modulus using an analytical model [30]; by using a local model based estimator of the impulse response of the shear-wave displacement curves [10]; and by using an analytical expression that is independent of shear-wave propagation model or viscoelastic model of the medium [31].

In this paper, we aim at characterizing tissue non-linear properties as a function of excitation frequency by simultaneously utilizing acousto-elasticity theory and spectral shear-wave elastography (SSWE). As it was theoretically shown in [32] that applying strains larger than a few percent is sufficient to perceive the influence of the fourth order elasticity constant, this parameter is also studied herein. For this purpose, incremental quasi-static external compressions (stresses) are applied to the tissue, while at each compression step measurements of SWS dispersion via SSWE are performed. Phantom and ex-vivo porcine liver studies are conducted herein to asses the feasibility of using this method to characterizing the non-linear parameters of tissue as a function of frequency. To our knowledge, this is the first study that uses shear-wave elastography to quantify non-linear properties of liver as a function of frequency.

II. Material and Methods

A. Data acquisition

In this work, the elastic parameters of tissue are determined from the propagation of induced shear-waves inside tissue, generated using a *supersonic shear-wave imaging* (SSI) technique [33]. SSI consists of two steps: Generation of shear-waves by using the radiation force from focused ultrasound beams (push mode) and high-speed (ultrafast) imaging of their propagation (imaging mode). A cylindrical shear-wave was generated using a push sequence, where three ultrasound beams are focused at 3 different points with a separation distance of 5 mm along the ultrasound transducer axis with a push duration of 100 μs. The resulting shear-wave is a broadband signal (50-1000 Hz).

A research ultrasound machine (Verasonics, Seattle, WA, USA) was used to program the transmit (Tx) sequence and to acquire raw receive (Rx) radio-frequency (RF) data for all transducer elements (channels) in parallel. Imaging was performed using a 128 linear-array transducer (Philips, ATL L7-4) at 5 MHz center frequency. After the ultrasound system is switched from push to imaging mode, the generated shear-waves were measured using high-speed plane wave imaging at a frame rate of 10 kHz. For improved accuracy with robustness to noise, images at three plane wave angles (-4,0,4 degrees) were collected alternately, with every three frames compounded before further processing.

A 1-D Cross correlation method [34] was used for estimating SWS from the particle velocity profiles obtained after using the 2D autocorrelator by Loupas et al. [35] on the acquired images. Estimated SWS is denoted with v_{g}, and referred to herein as group velocity of the shear-wave. Since this approach assumes a purely elastic medium, this group velocity encompasses in a single term the effect of all the frequency components of the shear-wave.

B. Shear-wave velocity dispersion

Tissue displacement fields $u(x, z, t)$ obtained from the procedure described above are used to extract the shear-wave phase velocity information. Estimating the frequency dependence of SWS is more difficult than estimating the group velocity, because the amount of energy for each frequency component is much smaller than the total energy of the signal. Therefore, a high measurement and tracking signal-to-noise ratio (SNR) is required. To achieve this, a trade-off between spatial resolution and SNR is achieved by averaging the tissue displacement fields along the axial direction, z, inside a region of interest (ROI). A schematic describing the procedure is illustrated in Fig. 1. An averaging window height between 2 mm and 10 mm was suggested in [36] and [26]. In this work, a ROI with a height of 5 mm was chosen. The resulting spatio-temporal map lateral direction. In a following step a 2D Fourier transform (2DFT) [28] is applied to the spatio-temporal map, which becomes a function of wavelength (λ) and temporal frequency (f), $U(\frac{1}{\lambda}, f)$. By finding for each temporal frequency the wavelength at which the FT amplitude is maximal, a frequency-dependent SWS can be reconstructed; as the phase velocity $v(f)$ at each frequency f. Since $v = \lambda f$, the phase velocity can be obtained by multiplying the spatial wavelength by the temporal frequency. As a confidence interval, the standard deviation of such phase velocity was also computed separately for several individual depths of the 5 mm ROI — as shown with the error-bars in the phase-velocity dispersion plot in Fig. 1.

C. Acousto-elasticity in nearly incompressible soft solids

In weakly non-linear isotropic elasticity theory, the strain energy density, W, can be expanded in terms of invariants of the Green-Lagrange strain tensor $\boldsymbol{E}$, i.e.

$$I_1 = tr(\boldsymbol{E}), I_2 = tr(\boldsymbol{E}^2), I_3 = tr(\boldsymbol{E}^3), \tag{1}$$

where tr is the trace and

$$\boldsymbol{E} = \frac{1}{2}(\boldsymbol{F}^T\boldsymbol{F} - I), \tag{2}$$

where $\boldsymbol{F}$ is the deformation gradient.

Considering an incompressible medium, Hamilton et. al [37] expanded the strain energy density up to fourth-order and showed that only three elastic constants are required for its characterization, i.e.

$$W = \mu I_2 + \frac{A}{3} I_3 + D I_2^2, \tag{3}$$

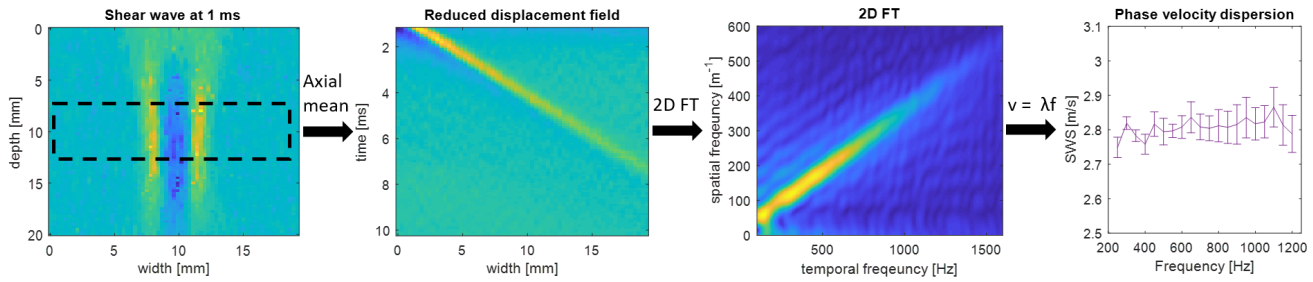

Fig. 1. Schematic describing the procedure to determine the dispersion curves for soft tissue. In a first step, averaging along the axial direction is performed to increase signal-to-noise (SNR), then a 2D Fourier transform is applied and finally the dispersion curve is reconstructed from the maxima of the 2D FT along each temporal frequency. Error-bars indicate the range of phase velocities computed separately for SWE at individual depths of the 5 mm ROI.

where I_2 and I_3 are the second and third-order Lagrangian strain invariants as defined in (1), μ is a Lamé parameter, A is the third oder elastic coefficeint as defined by Landau-Lifschitz, and D is the fourth order elastic coefficient as defined by Hamilton. These last three are, respectively, the second-, third-, and fourth-order elasticity constants of weakly non-linear incompressible isotropic elasticity. In this work to estimate these non-linear coefficients, AE measurements are performed on tissues, by applying varying stresses (preloads) on the target tissue and measuring the corresponding wave propagation speeds. A schematic describing the process can be seen in Fig. 2.

Considering only the first two terms of (3) for the strain energy density function and using the equations of motion for elastic waves in a uni-axially stressed solid, Gennisson et al. [15] derived the linear AE dependence of the squared wave speed on the uni-axial stress. For a shear-wave polarized along the axis of deformation (e.g. for the transducer generating the shear-waves placed along the applied uni-axial compression), they obtained

$$\rho v_{\mathrm{g}}^2 = \mu_0 - \sigma \frac{A}{12\mu_0}, \tag{4}$$

where μ_0 is the shear modulus in a stress free condition, A is the third order elastic constant, and σ is the applied stress and ρ is the tissue density. For homogeneous elastic materials, shear-wave velocity can be related to shear modulus as $\mu = \rho v^2$. Considering nearly-incompressible isotropic materials (i.e., Poisson's ratio ≈0.5), this yields to the relation for Young's modulus $E = 3\rho v^2$.

With the aforementioned assumptions of $\mu = \frac{1}{3}\frac{d\sigma}{d\epsilon}$, the stress at each compression step can be computed using

$$\sigma_i = \sigma_{i-1} + 3\mu_i(\epsilon_i - \epsilon_{i-1}), \tag{5}$$

with σ_0 being the stress at an initial loading step. For imaging using an ultrasound transducer that is barely in contact with tissue, a negligible stress (i.e. $\sigma_0 = 0\,Pa$) can be assumed. Using summation from zero loading to a given compression step, (5) can then be rewritten as

$$\sigma_i = \sum_{j=1}^{i} 3\mu_j(\epsilon_j - \epsilon_{j-1}). \tag{6}$$

Replacing (6) in (4) yields the SWS at each compression step as

$$\rho v_{gi}^2 = \mu_0 - [\sum_{j=1}^{i} 3\mu_j(\epsilon_j - \epsilon_{j-1})]\frac{A}{12\mu_0}, \tag{7}$$

which can be used to approximate (3) for small deformations, i.e. under small strain assumption, where the effect of the quadratic term and hence the elastic constant D in (3) would be negligible. The shear modulus at each compression step j was recovered from the shear wave speed measurement at that compression step, i.e. $\mu_j = \rho v_j^2$.

Considering larger deformations of tissues, all the terms in (3) should be taken into account. Relying on the large AE effect and starting from (3), Destrade et al. [32] related the squared wave speed of an infinitesimal wave traveling in an incompressible solid to the corresponding small-magnitude uni-axial pre-deformation. For a shear-wave polarized along the axis of deformation, they obtained:

$$\rho v_{\mathrm{g}}^2 = \mu_0 + (\frac{A}{4})\epsilon + (2\mu_0 + A + 3D)\epsilon^2, \tag{8}$$

with D the fourth order elastic constant– which does not appear in (7) under small strain assumption.

In this paper we will use both approaches above, i.e. equations (7) and (8), for investigating the non-linear parameter estimation. Note that parameter A can be estimated using both equations, while (8) in addition allows for estimating parameter D. We average the stress and strain values over the ROI, so these quantities throughout the rest of this paper should be interpreted as apparent stress and apparent strain.

D. Phantom Experiments

For validation of the proposed methods, a standard elasticity quality assurance phantom, CIRS 049 Elasticity QA, was used. This phantom is nearly-incompressible, has negligible viscosity, and has a background Young's modulus of 23 kPa around the homogeneous region it was imaged. The phantom experimental setup can be seen in Fig. 3(b). The imaging protocol described in Sec II-A was used for the purpose of characterizing the frequency dependent non-linearity of the phantom and for validation. To increase signal-to-noise ratio (SNR), the displacement fields from 10 consecutive SSWE acquisitions were averaged similarly to [26]. Using the 2D FT method in Sec. II-B, the shear-wave phase velocity was

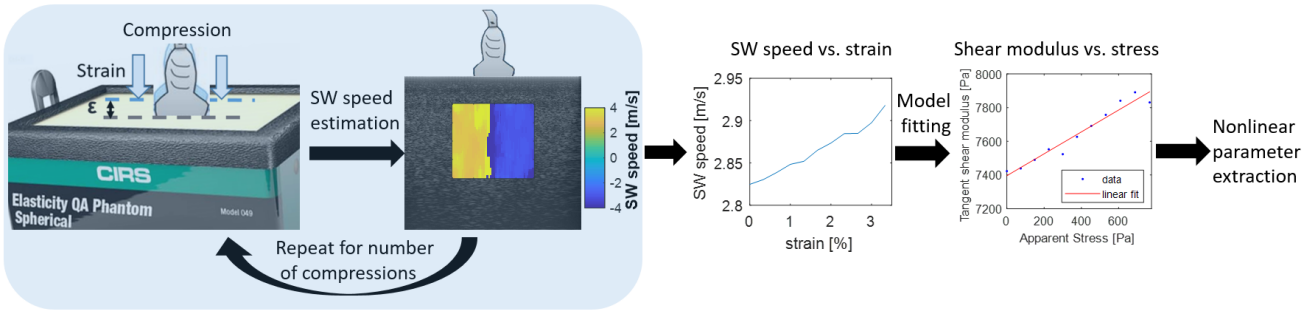

Fig. 2. Schematic illustrating the overall procedure of determining the non-linear parameters for soft tissue. From successive compressions and concurrent shear-wave measurements, *shear-modulus – stress* and *shear-modulus – strain* plots are computed. non-linear parameters can be extracted by fitting Eqs. (7) and (8) on these readings. Note that the displacement at the push location cannot be observed, so for the illustrative purposes of this figure such values were interpolated from surrounding readings.

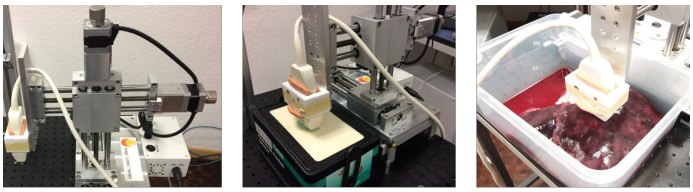

Fig. 3. Experimental setups: (a) Automated motorized linear-stage; (b) the experimental setup with the CIRS elastography phantom, (c) setup of ex-vivo experiments with livers placed on a flat plastic container surface.

computed. AE was then applied using successive compressions in steps (with a speed of 1 mm/s for each step) of 0.3 mm up to a total of 3 mm (corresponding to $\epsilon = 3.3\%$). To allow for tissue relaxation for a quasi-static assumption, we took the shear-wave measurements following a 1s delay after each compression step. A motorized 3-axis linear stage seen in Fig. 3(a) was used for accurate positioning and for repeatable compressions and measurements. Fitting the obtained phase velocity measurements to the non-linear models using (7) and (8) as in Sec. II-C, third and fourth order frequency dependent non-linear parameters A and D can be determined. In order to obtain a more stable parameter D, parameter A was first obtained by fitting (7) and it was kept fixed when subsequently fitting (8) to obtain D, as in [38]. Polynomial fitting using a least squares method from the curve fitting toolbox in Matlab was used to estimate these elastic parameters.

E. Ex-vivo liver study

To test the feasibility of using SSWE and AE for estimating the frequency dependent non-linear parameters of actual tissue, an ex-vivo study was performed on six porcine livers from a local slaughterhouse. The livers were placed in a plastic container that confined their motion in two lateral sides. The ex-vivo experimental setup is shown in Fig. 3(c). A similar procedure as described in II-D was used for data acquisition, however for an improved SNR in ex-vivo tissue, displacement fields from 30 consecutive SSWE acquisitions were averaged in these experiments prior to further processing, leading to an improvement of 12.6 dB. The SNR corresponding to 1, 10 and 30 average acquisitions was 11.4 dB, 20.3 dB and 24 dB. Compressions in steps of 0.5 mm up to a total of 5 mm were applied, corresponding to a strain of 12.5% to 15%, depending on the thickness of the particular liver sample. Third and fourth order non-linear parameters were determined in a consecutive order as described above in Sec. II-D.

F. Characterization of phantom and liver experiments

For all of the experimental results presented in this paper, the group velocity, v_{g}, was calculated as described in Sec. II-A using a cross correlation method on the displacement profile, $u(x, z, t)$, obtained from the 2D-Loupas correlator. Phase velocities, $v(f)$, were also computed by applying the 2D FT method in Sec. II-B (cf. Fig. 1) on the spatio-temporal map. In the following, our results will be described also in terms of phase velocity at the frequency corresponding to the center of gravity of the magnitude spectrum, using an approach similar to that described in [39]. A frequency-dependent weight corresponding to the absolute value of the FT was assigned for each frequency using

$$w(f) = |\mathcal{F}\{u(t)\}|, \tag{9}$$

where $w(x, f)$ is the weight corresponding to frequency f at position x. The center of gravity, denoted by f_{c}, is defined as [39]

$$f_{\mathrm{c}} = \frac{\sum f \cdot w(f)^2}{\sum w(f)^2}. \tag{10}$$

Then the phase velocity at the center of gravity, denoted by v_{c} is

$$v_{\mathrm{c}} = v(f_{\mathrm{c}}). \tag{11}$$

With the AE experiment, the SWS obtained at multiple compression levels can be used to extract the non-linear parameters. These parameters were determined by fitting corresponding models to the group, phase, and center of gravity phase velocity. The frequency-dependent non-linear parameters will be denoted as $A(f)$ and $D(f)$, the ones obtained from the group velocity as A_{g} and D_{g}, and those from the phase velocity at center of gravity as A_{c} and D_{c}.

G. Simulations

It was previously shown that the constitutive relation between loads (stresses) and deformations (strains) for liver parenchyma is non-linear and depends on the loading rate [40]. Additional complexity is introduced due to boundary conditions and non-homogeneous deformation distributions within the liver, thus the validation of the SWS values measured in experiments is important. For this purpose, the results presented in [23] on in-vivo liver mechanical characterization under different loading conditions using an aspiration device are compared to the ones presented in this paper. To do this, the model parameters extracted in [23] are used to simulate an experimental setup similar to ours.

3D simulations were performed with the finite element program Abaqus (Abaqus 6.10-EF1, DS Simulia Corp., Providence RI, USA). Geometrical dimensions were set based on the experiments. Two symmetry planes were introduced to quarter the computational field-of-view. Both liver and transducer were modeled as rectangular objects, with the liver being displacement-constrained on both lateral sides and left free on top and bottom sides with respect to the imaging plane, modeling the experimental setup. The transducer was modeled as a rigid body, while the liver parenchyma was represented with a hyperelastic incompressible material model (element type C3D8H) given by the volumetric strain-energy function (2nd order reduced polynomial):

$$W = C_{10}(I_1 - 3) + C_{20}(I_1 - 3)^2, \tag{12}$$

where C_{10} and C_{20} are model parameters and $I_1 = tr(\boldsymbol{F}\boldsymbol{F}^T)$. The interaction between transducer and parenchyma was modeled as frictionless in the tangential direction, and hard contact (displacement boundary) in the normal direction. Deformation dependent tangent stiffness arising from material non-linearity was extracted using the user output subroutine UVARM and the shear-wave speed was calculated as $v_g = \sqrt{\frac{E_{1212}}{\rho}}$, where ρ is the density that was assumed to be 1000 kg/m^3 (density of water) and E_{1212} is the tangent stiffness component relating the shear stress σ_{12} and the shear strain ϵ_{12}.

The mechanical behavior of the parenchyma is known to depend on the loading rate. The two extremes for the excitation timescale are quasi-static (qs) and quasi-instantaneous (qi), resulting in two different sets of model parameters as shown in [23] and presented in Table I. Global compression steps of the parenchyma with the transducer were considered quasi-static. Shear-wave excitation via acoustic radiation force is a transient, broad-band excitation, and thus is expected to behave somewhere between these two extremes (qs and qi). Thus, the tangent stiffness and the corresponding shear-wave speed were determined separately using both sets of model parameters in Table I, in order to analyze where our ex-vivo experimental lie with respect to these two extreme cases.

III. Results

A. Phantom results

CIRS phantom results are presented in Fig.4. The two dimensional velocity map that results from combining acousto-elasticity and spectroscopy, $v(f, \epsilon)$ is presented as a 1D function of frequency for several strain levels $\epsilon = \{0, 1, 2, 3\}$ % in Fig.4 (a), and as a function of strain for several frequencies $f = \{250, 500, 800, 1200\}$ Hz Fig.4 (b).

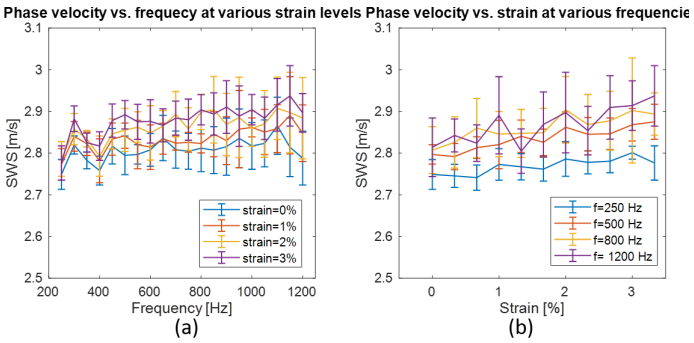

Fig. 4. Quantification of shear-wave speed variation with frequency (phase velocity) and amount of strain (non-linearity) on a CIRS quality assurance phantom with a theoretical background elasticity value of 2.77 m/s and a viscosity of 0 Pas, suggesting the phantom material to be relatively linear across frequencies. (a) shows phase velocities at strain levels of {0,1,2,3}%. (b) shows the AE effect at frequencies {250,500,800,1200} Hz. The error-bars represent the standard deviation of velocity estimates inside the measurement ROI.

The phantom properties specified by the manufacturer are Young modulus E=23 kPa, Poisson's ratio ν=0.5, density ρ=1000 kg/m^3, and viscosity η=0 Pas. From the given Young's modulus, we can infer the shear modulus $\mu = \frac{E}{2(1+\upsilon)} = 7.67$ kPa and expect the shear-wave speed $v_g = \sqrt{\frac{E}{3\rho}} = 2.77$ m/s.

Results in Fig.4 (a) indicate that the stress-free phase velocity ranges between 2.75 and 2.86 m/s, which is in agreement with the value specified by the manufacturer. A minor phase-velocity increase of $\approx 4 - 5\%/1000\,Hz$ is observed for any strain level, suggesting a minor viscous effect in the phantom. Similarly, from a zero strain condition to a strain level of 3.3%, only a minor SW group velocity increase of $\approx 2.5 - 4\%$ is observed regardless of frequency. For validation purposes, the phantom viscosity was estimated from the phase velocity dispersion using the Kelvin-Voigt spring-dashpot viscoelastic model by [41]

$$v(\omega) = \sqrt{\frac{2(\mu^2 + \omega^2\eta^2)}{\rho(\mu + \sqrt{\mu^2 + \omega^2\eta^2})}}, \tag{13}$$

which yields the negligible viscosity value of η=0.23 Pas for the phantom, corroborating with the manufacturer reported value.

Figure 5 illustrates the non-linear parameters of the CIRS phantom calculated after estimating v_g, $v(f)$, and v_c from

TABLE I
SIMULATION PARAMETER VALUES FOR QUASI-STATIC AND INSTANTANEOUS COMPRESSIONS.

	C_{10} [kPa]	C_{20} [kPa]
Quasi-static	0.7	4.5
Instantaneous	2.2	14.1

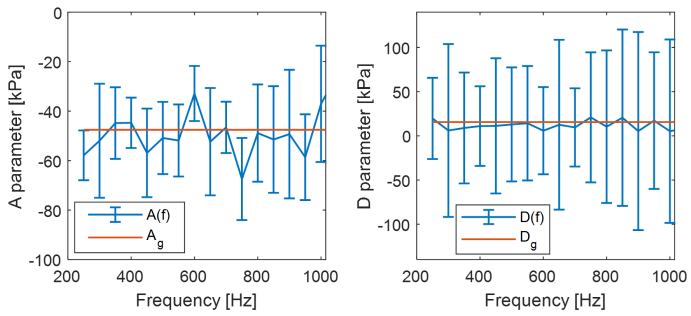

Fig. 5. Frequency-dependent non-linear parameters $A(f)$ and $D(f)$ (in blue) estimated in the background of the CIRS phantom with a known SWE of 2.77 m/s and viscosity of 0 Pas. A and D parameters extracted from the group velocity (v_g in red) are also shown for reference. The error-bars represent the 95% confidence interval range for the parameters.

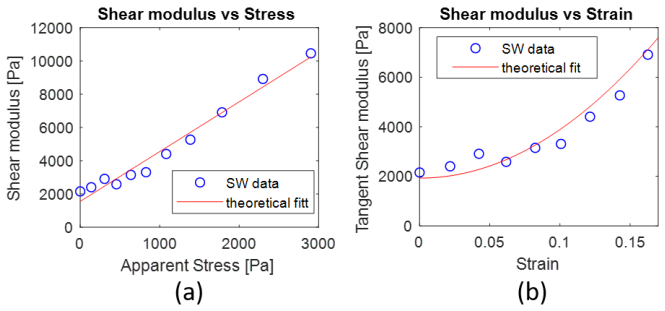

Fig. 6. non-linear parameter estimation for an ex-vivo porcine liver that was subjected to quasi-static compressions of 0.5 mm steps for a total of 5 mm ($\approx$ 14% strain). The A parameter is estimated first (a), using the measured shear-wave speeds in eq. (7), with D extracted from Eq. (8).

the shear-wave speeds obtained at multiple compression levels (strains) using (7) and (8). The error-bars in Fig. 5 represent the 95% confidence interval range of these non-linear parameters. Parameter A estimated from v_g, v_c, and $v(f)$ were, respectively, -48.9 kPa, -51.9 kPa and [-67.4, -32.9] kPa. Similarly, the estimated parameter D, respectively, were 23.5 kPa, 6.2 kPa, and [5.3, 21.1] kPa.

B. Ex-vivo liver study results

The feasibility of estimating the frequency dependent non-linear parameters of soft tissue using combined SSWE and AE was tested on six ex-vivo porcine livers, subjected to compressions corresponding to strain levels of 12-15%. Similar to Sec. II-D, the shear-wave speeds at different strains were used to extract the non-linear parameters. Parameter A is estimated by fitting the linear model (7) to the the tangent shear modulus–stress curve, as seen in Fig. 6(a). Parameter D is estimated by fitting the quadratic model (8) to the tangent shear modulus–strain curve as in Fig. 6(b).

Figure 7 shows the ex-vivo results of one porcine liver sample (#1) of 36 mm thickness, subjected to quasi-static compressions of 0.5 mm steps for a total of 5 mm ($\approx$14% strain). The velocity map is presented as a function of frequency at several strain levels $\epsilon = \{0, 4, 8, 12\}$ % in Fig. 7(a), and as a function of strain at several frequencies $f = \{100, 200, 400, 600\}$ Hz in Fig. 7(b). Results in Fig. 7(a) show an increase in phase velocity of $\approx 68-86\%/500$ Hz at any given strain level, suggesting a viscous medium. Using (13) and assuming a stress-free state, viscosity can be estimated as 1.3 Pas. Similarly, a shear-wave speed increase of $\approx 21-41\%$ can be observed for all frequencies at a strain level of 14%, suggesting a non-linear material. The group velocity is plotted in Fig. 7(c), with the upper and lower phase velocity limits of 100 Hz and 600 Hz shown with dashed lines and chosen as described in Section III-A. Figure 8 illustrates the non-linear parameters of the six ex-vivo porcine liver samples. A_g were in the range of [-127.7, -55.1] kPa with a mean value of -78.1 kPa, while A_c were in [-120.3, -43.8] kPa with a mean of -74.7 kPa. A large span of [-257, -26.1] kPa was obtained for the frequency dependent $A(f)$ parameter. A substantial change in $A(f)$ with frequency can be seen in Fig. 8 for all liver samples, with an increase of $\approx 12-33$ kPa/100 Hz. Similarly, D_g were in the range of [31.8, 110.0] kPa with a mean value of 53.2 kPa, while D_c were in [21.3, 109.4] kPa with a mean value of 49.9 kPa. A large span of [8.5, 252.4] kPa was obtained for the frequency dependent parameter $D(f)$. A substantial change in $D(f)$ with frequency is observed for all liver samples, with an increase of $\approx 10-38$ kPa/100 Hz.

All mechanical parameters for all liver samples are presented in Table II, together with their 95% confidence intervals.

C. Simulation Results

The mechanical simulation model and the results using the reduced polynomial model and the model parameters from Table I are presented in Fig. 9(a,b). Stress–strain curves are shown for quasi-static and quasi-instantaneous excitations, with an increase in stress observed for the latter case. These were then fitted using the models described in (7) and the non-linear parameter A was extracted from the quasi-static (qs) and quasi-instantaneous (qi) stress–strain plots, respectively, as A_{qs}=-34.5 kPa and A_{qi}=-101.9 kPa, with the error-bars in Fig. 9(c) showing the 95% confidence intervals. The simulation is used as a means to compare our (A) parameter range with those obtained in the in-vivo study [23], where a different model was used. Therefore, the simulation helped to interpret the model parameters used in our experiments in the context of the model (RP) parameters presented in [23] in a uniaxial experiment. In order to make a comparison with our ex-vivo experiments, we also placed in this figure the A values obtained from one liver sample. For this purpose, we picked our liver sample closest to that used earlier in [23] by choosing the one with a stress-free shear modulus value near the average of the shear-moduli of observed quasi-static and quasi-instantaneous simulations. This assumes the acoustic radiation force inducing a shear-wave excitation somewhere in the middle of quasi-static and quasi-instantaneous behaviours. For the simulations, one can estimate the quasi-static and quasi-instantaneous shear moduli algebraically from Table I using μ=$2C_{10}$, which leads to the stress-free values of $\mu_{0qs} = 1.4$ kPa and $\mu_{0qi} = 4.4$ kPa. The liver sample closest to their mean of 2.9 kPa is then sample #6. Accordingly, A_g from sample #6 is also shown in Fig. 9(c) to lie between the values

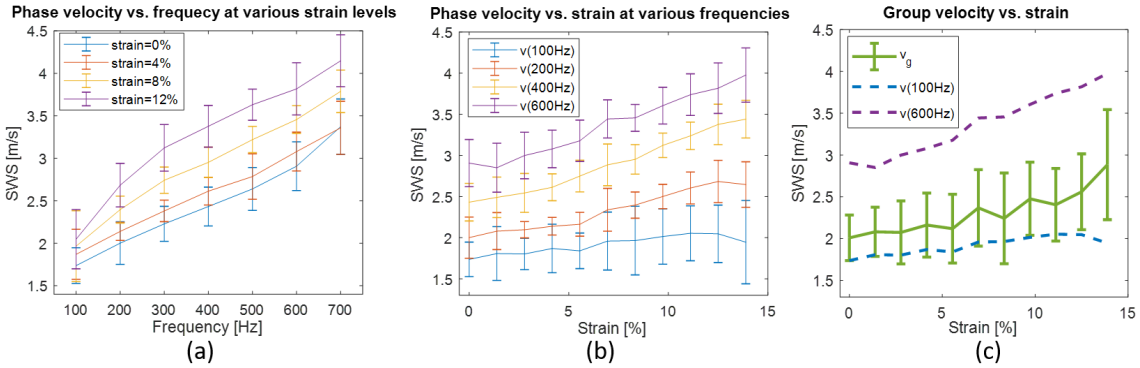

Fig. 7. Quantification of shear-wave speed variation with frequency (phase velocity) and amount of strain (non-linearity) on an ex-vivo porcine liver that was subjected to quasi-static compressions of 0.5 mm steps for a total of 5 mm ($\approx$ 14% strain). In (a) phase velocity at strain levels of $\{0,4,8,12\%\}$ are shown. The acousto-elasticity effect at frequencies of $\{100,200,400,600\,\text{Hz}\}$ is presented in (b).The error-bars represent the standard deviation of velocity estimates inside the ROI.

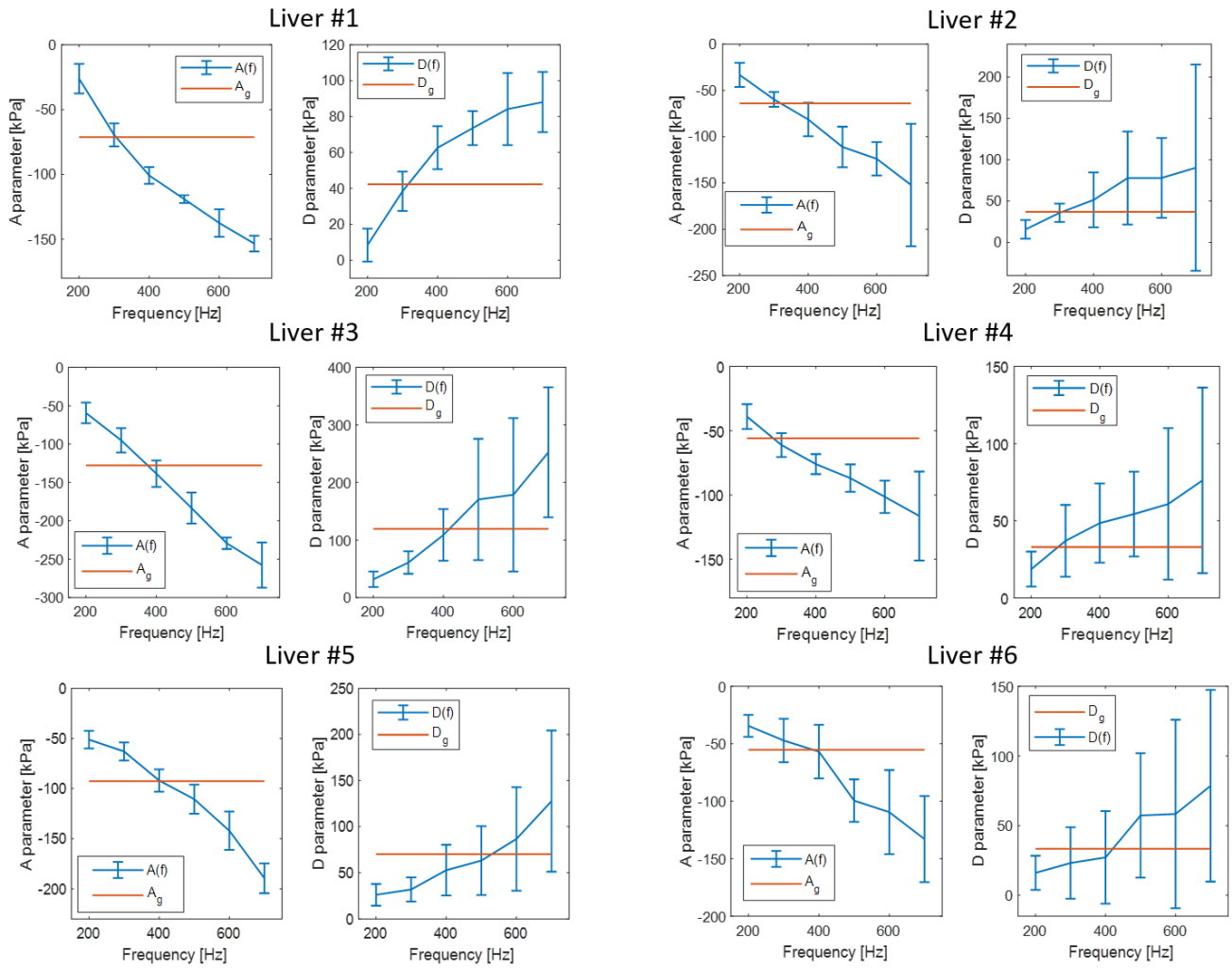

Fig. 8. Frequency dependent non-linear parameters A(f) and D(f) (in blue) extracted from 6 ex-vivo porcine livers that were subjected to quasi-static compressions of 0.5 mm steps for a total of 5 mm ($\approx$ 12-15% strain). A and D parameters extracted from the group velocity (v_g in red) are also shown for reference. Error-bars represent the 95% confidence interval range for the parameters.

TABLE II

ESTIMATED MECHANICAL PARAMETERS AND THEIR 95% CONFIDENCE INTERVAL RANGE (±) FOR THE CIRS PHANTOM AND THE EX-VIVO PORCINE LIVER SAMPLES. SHEAR MODULUS (μ_0) AND NON-LINEAR PARAMETERS A AND D WERE ESTIMATED FROM BOTH GROUP VELOCITY ($\cdot_g$), AND PHASE VELOCITY AT CENTER OF GRAVITY ($\cdot_c$) WHEREAS VISCOSITY (η) WAS ESTIMATED FROM THE DISPERSION CURVE AT STRESS-FREE STATE.

	μ_{0g} [kPa]	μ_{0c} [kPa]	A_g [kPa]	A_c [kPa]	D_g [kPa]	D_c [kPa]	η_0 [Pa s]
Phantom	7.9 ± 0.0	7.8 ± 0.0	-48.9 ± 20.2	-51.9 ± 23.6	23.5 ± 5.7	6.2 ± 93.2	0.2 ± 0.1
Liver #1	3.7 ± 0.6	3.7 ± 0.4	-71.3 ± 17.2	-73.6 ± 17.9	41.1 ± 25.6	46.6 ± 25.1	1.3 ± 0.2
Liver #2	3.5 ± 0.3	3.7 ± 0.4	-64.0 ± 7.2	-60.7 ± 9.7	35.6 ± 15.5	36.7 ± 11.7	1.4 ± 0.1
Liver #3	3.9 ± 0.3	3.7 ± 0.8	-127.7 ± 7.5	-120.3 ± 14.7	110.0 ± 6.3	109.4 ± 22.5	1.4 ± 0.3
Liver #4	3.0 ± 0.4	3.1 ± 0.3	-57.8 ± 9.7	-55.1 ± 9.8	31.8 ± 16.9	21.3 ± 21.1	1.0 ± 0.2
Liver #5	3.5 ± 0.2	4.7 ± 0.6	-92.6 ± 6.3	-94.2 ± 10.2	68.9 ± 10.1	57.3 ± 11.4	1.4 ± 0.2
Liver #6	2.8 ± 0.4	3.6 ± 0.7	-55.1 ± 6.2	-43.8 ± 18.4	32.3 ± 13.9	28.0 ± 11.2	1.2 ± 0.1

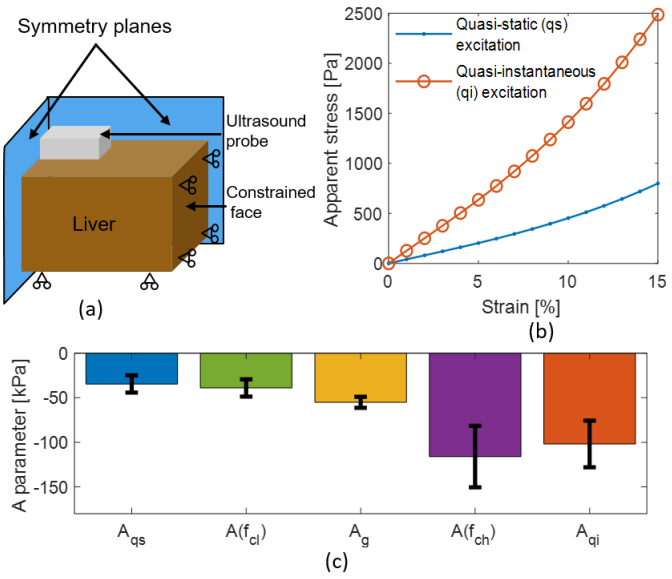

Fig. 9. (a) Simulation model (b) Stress-strain curves from simulations based on the reduced polynomial model for quasi-static (qs) and quasi-instantaneous (qi) excitation. (c) The non-linear parameter A estimated from simulations (A_{qs}, A_{qi}) in comparison with experimental group (A_{g}) and phase velocity ($A(f_{\mathrm{l}})$,$A(f_{\mathrm{u}})$) values for sample #6, where f_{l} and f_{u} are the lower and upper cut-off frequencies.

of A_{qs} and A_{qs}. Furthermore, as seen in Fig. 9(c), frequency-dependent parameter $A(f)$ estimated for #6 at the lower and upper frequency cut-off values do also lie within quasi-static and quasi-instantaneous extremes.

IV. DISCUSSION

Results indicate the feasibility of estimating frequency-dependent non-linear parameters using the proposed method, which could facilitate differentiation between tissue types. For the CIRS phantom, our estimations (v_{g}=2.82 m/s, η=0.23 Pas) strongly corroborate the manufacturer specified parameters (v=2.77 m/s, η=0 Pas), with the differences being < 0.05 m/s ($< 2\%$) for SW group velocity and 0.23 Pas for viscosity. The minor SW group velocity change of 0.12 m/s with frequency seen in Fig. 4(a) suggests that the phantom material is indeed non-dispersive. Similarly, we observe a small group velocity increase of 0.08 m/s (2.8%) for the applied strain range of 3.3%. It is worth mentioning that while standard deviations are large when compared to the overall increase in speed with frequency and strain in the phantom experiment from Fig. 4, similar standard deviation values were obtained in experimental studies in [26], [10]. This can be attributed to the noisy processes when computing the shear-wave speed for each frequency. However, owing to the multiple experimental repetitions performed, we do not expect this to change our conclusions.

To the best of our knowledge, ground-truth non-linear parameters for the particular CIRS phantom we used have not been reported in the literature, against which we can validate our results. Nevertheless, our estimated parameter A_{g}=−48.9 kPa is comparable to the non-linear parameters reported for similar synthetic phantoms: In [17], a mean value of -34.7±5.3 kPa for parameter A was reported across 5 phantoms. Our higher A parameter value can be explained by the higher shear modulus in our phantom ($\mu_{0\mathrm{g}}$=7.6 kPa) compared to theirs (μ_0=3.4 kPa).

Figure 5(a) shows a variation of the parameter A within a range of ±18 kPa around a mean point of 50 kPa. No significant trend being observed in this variation suggests that it is due to noise. This agrees with the large confidence intervals of ≈ ±20 kPa at each frequency. This corroborates the expectation of the phantom behaviour to be frequency-independent. A similar observation can also be made for parameter D in Fig. 5(b), with much larger confidence intervals of ≈ ± 90 kPa. This may be due to the stress applied on the phantom not being sufficiently large in order to accurately observe the fourth order elastic constant D, since very large stresses were avoided not to damage the phantom. Even so, no significant change in D was observed across frequencies.

These results obtained from applying AE and SSWE to the CIRS phantom indicate that it is possible to measure the frequency (in)dependent non-linear parameters using the proposed method. In the case of the CIRS phantom, where lateral stresses are present because of its containment in a box, the acousto-elasticity parameters approximated with a uniaxial stress assumption are accurate only within an error margin. Moreover, a small range of strain (3.3%) was applied to avoid phantom damage, which may have prohibited the observation of a non-linear response.

A close similarity between the group velocity and the phase velocity at the center of gravity was obtained for the

phantom experiments, with a difference of $< 2\%$. On the other hand, while still close, a larger difference of $5\% - 15\%$ was obtained for the ex-vivo liver experiments. Since the SW velocity is connected to the non-linear parameters, the same can be observed when comparing the difference between the parameter A based on group and phase velocity at center of gravity ($1 - 17\%$). As was shown in [10], this can be explained by the assumption of negligible viscosity when using a cross-correlation based method for estimating group velocity. The impact of viscosity on the cross-correlation group velocity estimation was shown in [10] to be more prominent at higher viscosity levels. This is due to frequency-dependent attenuation which causes lower frequencies, and implicitly the corresponding phase speeds, to become more dominant with the increase of distance from the source, distorting the shear-wave profile and introducing a bias. Due to the non-viscous nature of the phantom, where the SW velocity was relatively constant across frequencies, the shear-wave profile was distorted less, limiting such a bias above. The higher error-bars in the group velocity estimation compared to the phase velocity estimation can also be explained by this effect. Viscosity levels between 1-4 Pas were theoretically shown to increase the shear-wave speed estimation error between 4-7% when using the cross-correlation method. The 2D FT method, used for phase velocity estimation, was shown to have an error of only 1-3% for the same viscosity levels [10].

As opposed to the phantom case, the liver results from Fig. 7(a&b) show a larger increase in SW group velocity with frequency (1.5-2 m/s) and with strain (0.5-1 m/s), which are both to be expected for a viscous non-linear material such as liver. Due to the larger standard deviations seen in Fig. 7(b) at lower frequencies ($\leq$ 100 Hz) and at higher frequencies ($\geq$ 600 Hz), only the parameters within these intervals were displayed in Fig. 8.

Figure 8 reveals an increase in absolute value of both non-linear parameters with frequency, indicating that the non-linear effects elevate with frequency. There is certain variability in frequency response among the tested liver samples based on their estimated non-linear parameters A ($\approx 12 - 33$ kPa/100 Hz) and D ($\approx 10 - 38$ kPa/100 Hz.). The potential for these parameters being new mechanical biomarkers is to be further investigated, e.g. with controlled biological and/or chemical changes applied to tissues or with in-vivo studies with known pathological states. For instance, comparing A_{g} in the phantom (-48.9 kPa) and the liver sample #5 (-55.1 kPa), similar values can be observed with highly overlapping confidence interval bounds. However, by looking at the frequency dependent parameter $A(f)$, a clear distinction between these two can be made, cf. Fig. 10(a). A similar differentiation can be made also between liver samples #1 and #4, based on the variation $A(f)$, cf. Fig. 10(b). Whether this difference has clinical relevance should be the subject of further study.

As seen in Fig. 9(c), the parameters estimated from the ex-vivo samples exhibit a good agreement with the parameters estimated from the 3D finite-element simulations based on the parameters with an aspiration device presented in [23]. Similar ranges for the parameter A can be observed between the simulations ([-101.9, -34.5] kPa) and the experimental results ([-116.1, -39] kPa). A larger upper limit (i.e. absolute value) would be expected from the simulations for the quasi-instantaneous response case when compared to the experimental results. This can be attributed to the fact that in the work of [23], on which our simulations are based, the quasi-instantaneous response parameters were measured in in-vivo mechanical tests. Therefore the strain rates (and frequency response) were limited because of physical constraints and hence a true quasi-instantaneous response was not measured. The actual strain rates in their experiments were $\approx$1–3 mm$\cdot$ s^{-1}, comparable to the ones induced in our shear-wave experiments of $\approx$0.5–1 mm$\cdot$ms^{-1}.

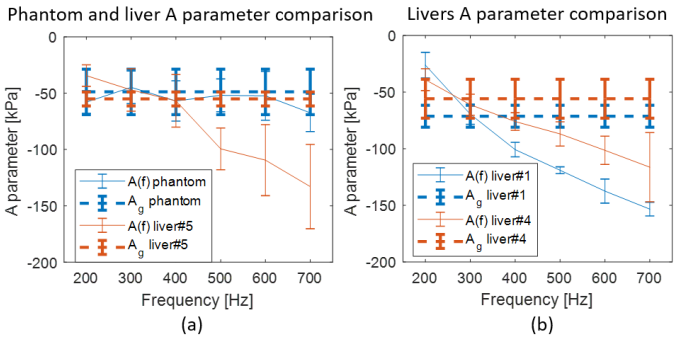

Fig. 10. Comparison of group velocity based (A_{g}) and frequency-dependent ($A(f)$) parameter: (a) between CIRS phantom and the sample #5, and (b) between liver samples #1 and #4.

The stress free shear modulus ([2.8, 3.9] kPa) and viscosity ([1.03, 1.43] Pas) values obtained in our liver study were similar to other values reported in the literature. Porcine liver studies performed in [42] using multiple harmonic excitations, revealed a mean shear modulus of 2.2 kPa and viscosity of 1.8 Pas. Studies in [41] using shear-wave dispersion ultrasound vibrometry resulted in a mean shear modulus of 5.4 kPa and viscosity of 1.43 Pas. Third order non-linear parameters have been previously studied in the literature [16], [17] however not on porcine but bovine liver pieces embedded in gelatin blocks. In [16] the parameter A was estimated in the range of [-576, -128] kPa with a mean value of -335 kPa using SSI and a large rigid compression plate. Values closer to ours were obtained in [17], with A within [-115, -98] kPa with a mean of -114 kPa, also using SSI but with a smaller compression plate attached to the transducer. While the results are similar, there could be several reasons for the differences to the parameters in our experiments (A=[-128, -55], mean of -78 kPa). Our measurements were performed on whole livers as opposed to small liver pieces (1-2 cm^3) embedded in gelatin. Moreover, it was shown in [19] that differences of up to 50% in the parameter A measurement may occur from using a compression plate of 11.5$\times$4.5 cm as opposed to only using the ultrasound probe for compression. This is because the different stress distributions do not fulfill the uni-axial stress assumption in the latter case. To our knowledge, the fourth order parameter D has not been investigated on liver in the literature before. A study on porcine brains in [22] revealed a mean D of 5.8 ± 1.4 kPa and A of -13.6 ± 7.1 kPa,

which would confirm that brain tissue is significantly more linear than liver. The large difference in A parameters (from highly non-linear towards more linear) between bladder [18], liver [17], kidney [19] and brain [22] show the importance of non-linear parameters in tissue. On the other hand, we have shown that there is a significant variation of these parameters with frequency. Because of this, it is not possible to accurately quantify tissue non-linearity between ultrasound equipments that provide different excitation frequencies or bandwidths. For this reason, our work proposes the study of non-linear parameters in a frequency dependent manner. The model used in this manuscript is based on the assumption of a nonlinear but purely elastic material. Since tissues are not homogeneous, but instead contain micro structures at multiple scales (e.g., cells, fibers, vessels, etc), waves at different frequencies may "see" different such structures and thus encounter different nonlinear responses. Accordingly, tissues are known to exhibit dispersive effects. Often, the choice of material model is a trade-off between accuracy (for representativeness) and simplicity (for robustness) for a given measurement setting and application scenario. There have been various studies, where the elastic model was based on (3) [15], [16], [17], [18], [19], or on a plethora of other different (hyperelastic) models [43], [21], for describing the behaviour of dispersive tissue. Herein we estimate tissue nonlinear parameters as a function of frequency of the applied stress, where a wide range of variation is observed. These are argued to be potentially beneficial for tissue differentiation. Nevertheless, the mechanisms leading to these differences are not herein investigated, i.e. if mode conversion or attenuation at different frequencies may play a role in the observations. One limitation of this method is that the estimation of non-linear parameters using (7) and (8) relies on the application of uni-axial stress. In clinical scenarios, this can be challenging due to the tissue geometry and the depth of target tissue inside the body. This variation of the estimated non-linear parameters in the presence and absence of a compression plate was studied in [19]. Note that with the ROI based estimation of shear-wave phase velocity, we achieve quantification with a ROI but without any spatial variation. Alternatively, a point based estimation can be adopted for better spatial distribution, similarly to [10]. While whole livers were used in our study, a possible limitation is the lack of liver perfusion and pressurization as encountered in in-vivo cases, which could alter the non-linear parameters. In future work, healthy and pathological livers shall be investigated to asses the importance of frequency based non-linear parameters as a potential biomarker.

V. CONCLUSIONS

In this work, a study on extracting frequency dependent non-linear parameters has been presented using shear-wave elastography and quasi-static compressions. Thanks to the broadband characteristics of the induced shear-wave, shear-wave spectroscopy could be coupled with acousto-elasticity measurements giving access to frequency- and strain-dependent shear-wave measurements. By fitting these to mathematical models, frequency-dependent parameters were obtained. Results on a CIRS elastography phantom revealed no significant change in elastic parameters with frequency, confirming the linear behavior of the phantom. A study with 6 ex-vivo porcine livers with dispersion characteristics has revealed a significant variation in both non-linear parameters A and D with frequency. Frequency-independent group velocity and center of gravity phase velocity parameters were computed. These have demonstrated a good agreement and were both within the limits determined by the upper and lower boundaries of the frequency dependent parameters.

We have demonstrated that it is possible to estimate frequency dependent non-linear parameters using the proposed method, with the estimated group velocity parameter values being in agreement with those reported previously in the literature. The measurement technique can be applied to different body areas and disease entities using a conventional ultrasound machine. It has potential to add further information to the detection and characterization of diseases.

ACKNOWLEDGMENT

This work was supported by the Swiss National Science Foundation (SNSF) and a Hochschulmedizin Zurich (HMZ) Seed Grant. We thank Kevin Bircher for the numerical simulations, and Prof. Edoardo Mazza for the discussions on mechanical characterization, experimental design, and the results.

REFERENCES

[1] T. Deffieux, J.-L. Gennisson, L. Bousquet, M. Corouge, S. Cosconea, D. Amroun, S. Tripon, B. Terris, V. Mallet, and P. Sogni, "Investigating liver stiffness and viscosity for fibrosis, steatosis and activity staging using shear wave elastography," *Journal of Hepatology*, vol. 62, no. 2, pp. 317–324, 2015.

[2] C. T. Barry, B. Mills, Z. Hah, R. A. Mooney, C. K. Ryan, D. J. Rubens, and K. J. Parker, "Shear wave dispersion measures liver steatosis," *Ultrasound in Medicine & Biology*, vol. 38, no. 2, pp. 175–182, 2012.

[3] T. A. Krouskop, T. M. Wheeler, F. Kallel, B. S. Garra, and T. Hall, "Elastic moduli of breast and prostate tissues under compression," *Ultrasonic Imaging*, vol. 20, no. 4, pp. 260–274, 1998.

[4] K. V. Ramnarine, J. W. Garrard, K. Dexter, S. Nduwayo, R. B. Panerai, and T. G. Robinson, "Shear wave elastography assessment of carotid plaque stiffness: in vitro reproducibility study," *Ultrasound in Medicine & Biology*, vol. 40, no. 1, pp. 200–209, 2014.

[5] T. Shiina, K. R. Nightingale, M. L. Palmeri, T. J. Hall, J. C. Bamber, R. G. Barr, L. Castera, B. I. Choi, Y.-H. Chou, D. Cosgrove *et al.*, "WFUMB guidelines and recommendations for clinical use of ultrasound elastography: Part 1: basic principles and terminology," *Ultrasound in Medicine & Biology*, vol. 41, no. 5, pp. 1126–1147, 2015.

[6] A. P. Sarvazyan, O. V. Rudenko, S. D. Swanson, J. B. Fowlkes, and S. Y. Emelianov, "Shear wave elasticity imaging: a new ultrasonic technology of medical diagnostics," *Ultrasound in Medicine & Biology*, vol. 24, no. 9, pp. 1419–1435, 1998.

[7] M. Tanter, J. Bercoff, A. Athanasiou, T. Deffieux, J.-L. Gennisson, G. Montaldo, M. Muller, A. Tardivon, and M. Fink, "Quantitative assessment of breast lesion viscoelasticity: initial clinical results using supersonic shear imaging," *Ultrasound in Medicine & Biology*, vol. 34, no. 9, pp. 1373–1386, 2008.

[8] M. Y. Kim, N. Choi, J.-H. Yang, Y. B. Yoo, and K. S. Park, "False positive or negative results of shear-wave elastography in differentiating benign from malignant breast masses: analysis of clinical and ultrasonographic characteristics," *Acta Radiologica*, vol. 56, no. 10, pp. 1155–1162, 2015.

[9] M. L. Palmeri, B. Qiang, S. Chen, and M. W. Urban, "Guidelines for finite-element modeling of acoustic radiation force-induced shear wave propagation in tissue-mimicking media," *IEEE Trans Ultrasonics, Ferroelectrics, and Frequency Control*, vol. 64, pp. 78–92, 2017.

[10] R. J. van Sloun, R. R. Wildeboer, H. Wijkstra, and M. Mischi, "Viscoelasticity mapping by identification of local shear wave dynamics," *IEEE Trans Ultrasonics, Ferroelectrics, and Frequency Control*, vol. 64, no. 11, pp. 1666–1673, 2017.

[11] K. R. Nightingale, N. C. Rouze, S. J. Rosenzweig, M. H. Wang, M. F. Abdelmalek, C. D. Guy, and M. L. Palmeri, "Derivation and analysis of viscoelastic properties in human liver: impact of frequency on fibrosis and steatosis staging," *IEEE Trans Ultrasonics, Ferroelectrics, and Frequency Control*, vol. 62, no. 1, p. 165, 2015.

[12] M. B. Rominger, P. Kälin, M. Mastalerz, K. Martini, V. Klingmüller, S. Sanabria, and T. Frauenfelder, "Influencing factors of 2D shear wave elastography of the muscle–an ex vivo animal study," *Ultrasound International Open*, vol. 4, no. 02, pp. E54–E60, 2018.

[13] P. Wellman, R. D. Howe, E. Dalton, and K. A. Kern, "Breast tissue stiffness in compression is correlated to histological diagnosis," *Harvard BioRobotics Laboratory Technical Report*, pp. 1–15, 1999.

[14] S. Goenezen, P. Barbone, and A. A. Oberai, "Solution of the nonlinear elasticity imaging inverse problem: The incompressible case," *Computer methods in applied mechanics and engineering*, vol. 200, no. 13, pp. 1406–1420, 2011.

[15] J.-L. Gennisson, M. Rénier, S. Catheline, C. Barrière, J. Bercoff, M. Tanter, and M. Fink, "Acoustoelasticity in soft solids: Assessment of the nonlinear shear modulus with the acoustic radiation force," *The Journal of the Acoustical Society of America*, vol. 122, no. 6, pp. 3211–3219, 2007.

[16] H. Latorre-Ossa, J.-L. Gennisson, E. De Brosses, and M. Tanter, "Quantitative imaging of nonlinear shear modulus by combining static elastography and shear wave elastography," *IEEE Trans Ultrasonics, Ferroelectrics, and Frequency Control*, vol. 59, no. 4, pp. 833–839, 2012.

[17] M. Bernal, F. Chamming's, M. Couade, J. Bercoff, M. Tanter, and J.-L. Gennisson, "In vivo quantification of the nonlinear shear modulus in breast lesions: feasibility study," *IEEE Trans Ultrasonics, Ferroelectrics, and Frequency Control*, vol. 63, no. 1, pp. 101–109, 2016.

[18] M. Bayat, A. Singh, J. Webb, V. Kumar, A. Gregory, A. Alizad, and M. Fatemi, "Acoustoelasticity modeling of bladder tissue nonlinearity: Ex vivo study," in *Ultrasonics Symposium (IUS), 2017 IEEE International*. IEEE, 2017, pp. 1–4.

[19] S. Aristizabal, C. A. Carrascal, I. Z. Nenadic, J. F. Greenleaf, and M. W. Urban, "Application of acoustoelasticity to evaluate nonlinear modulus in ex vivo kidneys," *IEEE Trans Ultrasonics, Ferroelectrics, and Frequency Control*, vol. 65, no. 2, pp. 188–200, 2018.

[20] L. Landau, E. Lifshitz, A. Kosevich, and L. Pitaevskii, "Theory of elasticity (3rd english ed.) pergamon press," 1986.

[21] Y. Jiang, G.-Y. Li, L.-X. Qian, X.-D. Hu, D. Liu, S. Liang, and Y. Cao, "Characterization of the nonlinear elastic properties of soft tissues using the supersonic shear imaging (ssi) technique: inverse method, ex vivo and in vivo experiments," *Medical image analysis*, vol. 20, no. 1, pp. 97–111, 2015.

[22] Y. Jiang, G. Li, L.-X. Qian, S. Liang, M. Destrade, and Y. Cao, "Measuring the linear and nonlinear elastic properties of brain tissue with shear waves and inverse analysis," *Biomechanics and modeling in mechanobiology*, vol. 14, no. 5, pp. 1119–1128, 2015.

[23] M. W. Hollenstein, "Mechanics of the human liver: experiments and modeling," Ph.D. dissertation, ETH Zurich, 2011.

[24] J. G. Snedeker, P. Niederer, F. Schmidlin, M. Farshad, C. Demetropoulos, J. Lee, and K. Yang, "Strain-rate dependent material properties of the porcine and human kidney capsule," *Journal of Biomechanics*, vol. 38, no. 5, pp. 1011–1021, 2005.

[25] S. Chen, M. W. Urban, C. Pislaru, R. Kinnick, Y. Zheng, A. Yao, and J. F. Greenleaf, "Shearwave dispersion ultrasound vibrometry (SDUV) for measuring tissue elasticity and viscosity," *IEEE Trans Ultrasonics, Ferroelectrics, and Frequency Control*, vol. 56, no. 1, pp. 55–62, 2009.

[26] T. Deffieux, G. Montaldo, M. Tanter, and M. Fink, "Shear wave spectroscopy for in vivo quantification of human soft tissues viscoelasticity," *IEEE transactions on medical imaging*, vol. 28, no. 3, pp. 313–322, 2009.

[27] M. Bernal, I. Nenadic, M. W. Urban, and J. F. Greenleaf, "Material property estimation for tubes and arteries using ultrasound radiation force and analysis of propagating modes," *The Journal of the Acoustical Society of America*, vol. 129, no. 3, pp. 1344–1354, 2011.

[28] I. Z. Nenadic, M. W. Urban, H. Zhao, W. Sanchez, P. E. Morgan, J. F. Greenleaf, and S. Chen, "Application of attenuation measuring ultrasound shearwave elastography in 8 post-transplant liver patients," in *Ultrasonics Symposium (IUS), 2014 IEEE International*. IEEE, 2014, pp. 987–990.

[29] M. R. Selzo and C. M. Gallippi, "Viscoelastic response (visr) imaging for assessment of viscoelasticity in voigt materials," *IEEE Trans Ultrasonics, Ferroelectrics, and Frequency Control*, vol. 60, no. 12, p. 2488, 2013.

[30] S. Kazemirad, S. Bernard, S. Hybois, A. Tang, and G. Cloutier, "Ultrasound shear wave viscoelastography: Model-independent quantification of the complex shear modulus," *IEEE Trans Ultrasonics, Ferroelectrics, and Frequency Control*, vol. 63, no. 9, pp. 1399–1408, 2016.

[31] K. J. Parker, J. Ormachea, S. Will, and Z. Hah, "Analysis of transient shear wave in lossy media," *Ultrasound in Medicine & Biology*, vol. 44, no. 7, pp. 1504–1515, 2018.

[32] M. Destrade, M. D. Gilchrist, and G. Saccomandi, "Third-and fourth-order constants of incompressible soft solids and the acousto-elastic effect," *The Journal of the Acoustical Society of America*, vol. 127, no. 5, pp. 2759–2763, 2010.

[33] J. Bercoff, M. Tanter, and M. Fink, "Supersonic shear imaging: a new technique for soft tissue elasticity mapping," *IEEE Trans Ultrasonics, Ferroelectrics, and Frequency Control*, vol. 51, no. 4, pp. 396–409, 2004.

[34] C. Kasai, K. Namekawa, A. Koyano, and R. Omoto, "Real-time two-dimensional blood flow imaging using an autocorrelation technique," *IEEE Transactions on sonics and ultrasonics*, vol. 32, no. 3, pp. 458–464, 1985.

[35] T. Loupas, J. Powers, and R. W. Gill, "An axial velocity estimator for ultrasound blood flow imaging, based on a full evaluation of the doppler equation by means of a two-dimensional autocorrelation approach," *IEEE Trans Ultrasonics, Ferroelectrics, and Frequency Control*, vol. 42, no. 4, pp. 672–688, 1995.

[36] J. Brum, M. Bernal, J. Gennisson, and M. Tanter, "In vivo evaluation of the elastic anisotropy of the human achilles tendon using shear wave dispersion analysis," *Physics in Medicine & Biology*, vol. 59, no. 3, p. 505, 2014.

[37] M. F. Hamilton, Y. A. Ilinskii, and E. A. Zabolotskaya, "Separation of compressibility and shear deformation in the elastic energy density (l)," *The Journal of the Acoustical Society of America*, vol. 116, no. 1, pp. 41–44, 2004.

[38] C. F. Otesteanu, B. R. Chintada, S. J. Sanabria, M. Rominger, E. Mazza, and O. Goksel, "Quantification of nonlinear elastic constants using polynomials in quasi-incompressible soft solids," in *Ultrasonics Symposium (IUS), 2017 IEEE International*. IEEE, 2017, pp. 1–4.

[39] C. Amador, M. W. Urban, S. Chen, Q. Chen, K.-N. An, and J. F. Greenleaf, "Shear elastic modulus estimation from indentation and sduv on gelatin phantoms," *IEEE Transactions on Biomedical Engineering*, vol. 58, no. 6, pp. 1706–1714, 2011.

[40] A. Nava, E. Mazza, M. Furrer, P. Villiger, and W. Reinhart, "In vivo mechanical characterization of human liver," *Medical image analysis*, vol. 12, no. 2, pp. 203–216, 2008.

[41] K. Chen, A. Yao, E. E. Zheng, J. Lin, and Y. Zheng, "Shear wave dispersion ultrasound vibrometry based on a different mechanical model for soft tissue characterization," *Journal of Ultrasound in Medicine*, vol. 31, no. 12, pp. 2001–2011, 2012.

[42] M. Orescanin, M. A. Qayyum, K. S. Toohey, and M. F. Insana, "Dispersion and shear modulus measurements of porcine liver," *Ultrasonic imaging*, vol. 32, no. 4, pp. 255–266, 2010.

[43] J. Jiang, T. Varghese, C. L. Brace, E. L. Madsen, T. J. Hall, S. Bharat, M. A. Hobson, J. A. Zagzebski, and F. T. Lee, "Young's modulus reconstruction for radio-frequency ablation electrode-induced displacement fields: a feasibility study," *IEEE Trans. Med. Imag.*, vol. 28, no. 8, pp. 1325–1334, 2009.